ARTICLE

Observation of a robust catalyst support based on metallic glass for large current-density water electrolysis

Received 00th January 20xx,
Accepted 00th January 20xx

DOI: 10.1039/x0xx00000x

Mengqi Pan[a,b], Heyang Feng[a], Ziyong Zhang[a], Meng Gao[a,b], Lei Lei[c], Degao Wang[c], Guowei Li[a*], Juntao Huo[a,b*], Jun-Qiang Wang[a,b*]

Support materials such as activated carbon are essential for electrochemical heterogeneous reactions, providing a stable matrix for metal catalysts and actively influencing the catalyst's properties and effectiveness. Although various effective carbon supports have been commercially developed, corrosion and catalyst degradation are still inevitable under high current density catalysis, for instance, during the harsh alkaline water electrolysis process. Here, we report the synthesis of a new type of metallic glass (MG) support through the deployment of an amorphous alloy with tunable Pt loading mass ($Fe_{70-x}Co_{10}Ni_{10}Zr_{10}Pt_x$, x = 1, 3, 5). In addition to the advantages of high specific surface areas and enhanced chemical stability, X-ray absorption spectroscopy and theoretical investigations suggest that the MG support could modulate the electronic structure of Pt active sites through strong metal-support interaction, leading to the enhanced water dissociation kinetics. When compared with those previously reported carbon-supported or pure Pt catalysts, the MG-supported catalysts exhibit remarkably high activities towards hydrogen evolution, which only requires an overpotential of 102 mV at the current density of 1000 mA cm^{-2} with a Faraday efficiency close to 100%. This allows the current density to be increased to 500 mA cm^{-2} during the stability test without corrosion and degradation. We argue that the earth-abundant elements-based MG support could be an alternative for metal catalysts that can withstand the physical and chemical corrosion encountered during harsh catalytic reactions.

Introduction

Identifying and developing high-performance metal catalysts is important for chemical reactions that solve energy and environmental problems, from green hydrogen production to fuel cells and carbon capture applications.[1-5] Support materials with high surface areas and good conductivity are indispensable elements for the functions of the metal catalysts, providing a vast surface for dispersion and facilitating rapid electron transfer to and from the catalytic active sites.[6-10] Compounds based on *p*-block elements continue to be the most commonly used supports, including activated carbon, carbon black, graphene, nitrogen-doped carbon, or boron nitride.[11] Although such carbon-supported catalysts exhibit high performance in various applications such as water splitting, it remains a challenge to further enhance the efficiencies and overcome the stability issues.[12-14] Under harsh catalytic conditions of high-current density and prolonged operation, carbon support corrosion will occur within the catalyst layers, leading to the dissolution, agglomeration, and Ostwald ripening of the metal catalysts.[15, 16] This results in the decrease of the electrochemical surface areas and is detrimental to both the activity and stability of the catalysts.[12, 13, 15] Furthermore, since most metal catalysts are deposited onto the supports with weak interaction, it is difficult to modulate the electronic structures of Pt through metal-support interaction.[17, 18] Thus, the optimization of the structural configuration of metallic catalysts and the selection of robust support materials equally important in the search for catalysts that work under large current densities.

Metallic glass (MG), a type of alloy where atoms are arranged in a topologically disordered manner in three dimensions, exhibits a more homogeneous structure and superior mechanical properties compared to its crystalline counterparts.[19-22] This unique arrangement of atoms contributes to its candidacy as a material for self-supporting electrodes due to its wide compositional flexibility, uniform elemental distribution within the alloy, and stable chemical bonding structure between atoms.[23-26] The preparation of Pt-loaded MG ribbons can address a series of challenges commonly associated with carbon-loaded catalysts, such as the state-of-the-art commercial Pt/C catalyst.[27] In MG support, platinum that is chemically bonded exhibits greater stability than the physically adsorbed metal catalysts on various carbon supports.[28, 29] This stability ensures that the active sites are less prone to dissolution and degradation over time, enhancing the

[a] *CAS Key Laboratory of Magnetic Materials and Devices, and Zhejiang Province Key Laboratory of Magnetic Materials and Application Technology, Ningbo Institute of Materials Technology and Engineering, Chinese Academy of Sciences, Ningbo, China. liguowei@nimte.ac.cn; huojuntao@nimte.ac.cn; wangjunqiang@nimte.ac.cn;*
[b] *Center of Materials Science and Optoelectronics Engineering, University of Chinese Academy of Sciences, Beijing, China;*
[c] *Zhejiang Key Laboratory of Data-Driven High-Safety Energy Materials and Applications Ningbo Institute of Materials Technology and Engineering, Chinese Academy of Sciences, Ningbo, China.*
Electronic Supplementary Information (ESI) available: Experimental section, Fig. S1-S25, Table S1-S7. See DOI: 10.1039/x0xx00000x

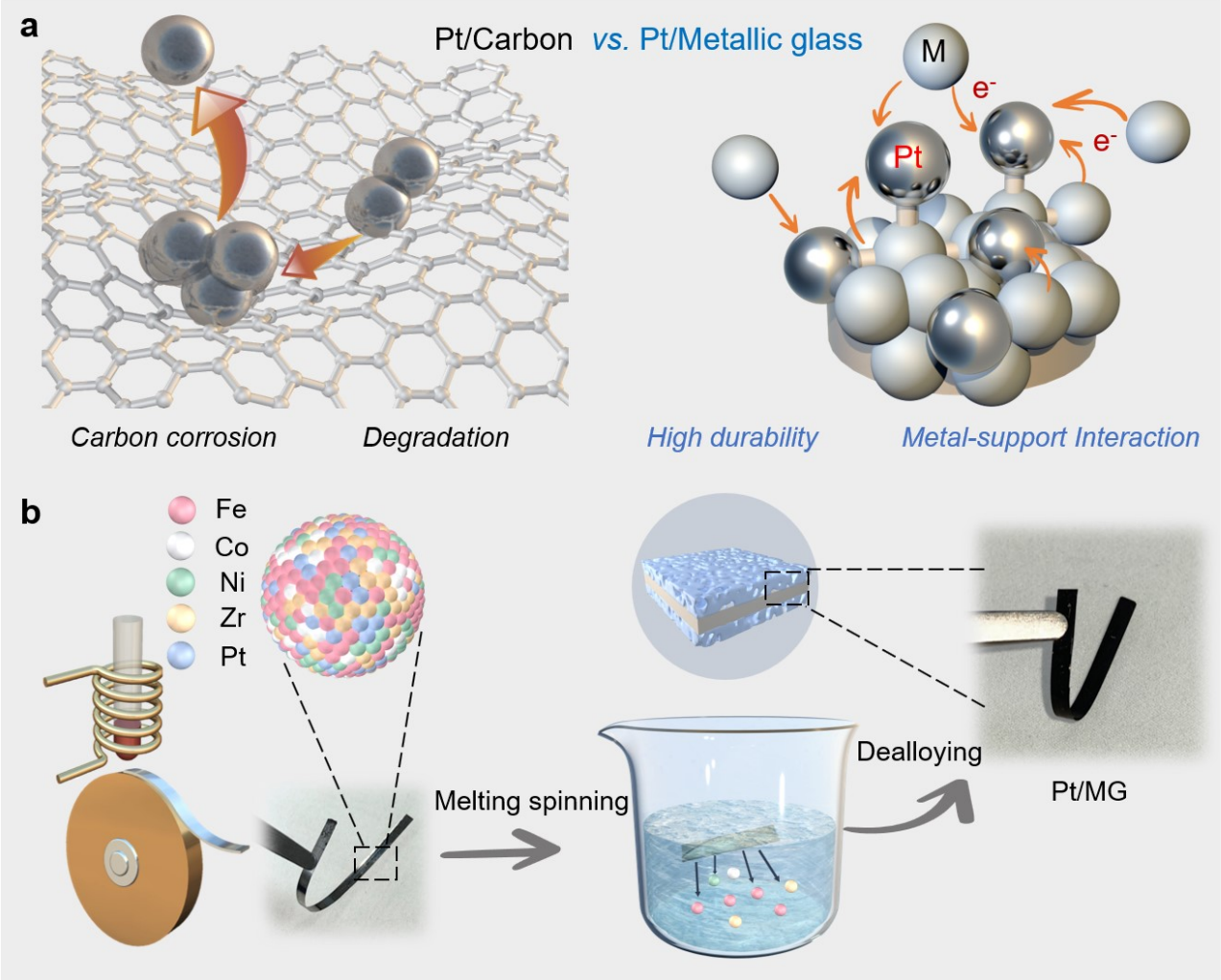

Fig. 1 (a) Comparison between carbon-supported and metallic glass-supported catalysts. (b) Schematic illustration of the preparation process of the Pt/MG catalysts.

longevity and efficacy of the catalyst.[30] MG catalysts containing precious metals such as PdNiCuP,[31] PdPtCuNiP,[32] AlNiCoMnYAu,[24] ZrNiTiPt,[30] *etc.* have good catalytic properties. However, these catalysts typically incorporate substantial quantities of precious metals and their stability has been examined only at low current densities, which is insufficient to meet industrial-scale requirements.[33] The synthesis of low-cost catalysts that maintain robust stability at high current densities (such as 500 mA cm^{-2}) is an imperative issue that needs to be addressed currently.[34-37] Additionally, studies on the mechanism by which MG, as supports, affect the catalytic properties of the loaded precious metals are scarce and require further investigation.

In this study, the FeZr system, known for its high amorphous formation ability, was selected to explore its potential as a support for noble metal catalysts. The aim is to guide the design of high-performance catalysts for alkaline water electrolysis.[38] Co and Ni elements with lower electronegativity were selected to facilitate electronic structure tuning.[13, 39] $Fe_{70-x}Co_{10}Ni_{10}Zr_{10}Pt_x$ (x=0, 1, 3, 5) amorphous alloy precursors (MG ribbon) with different Pt contents were synthesized by the melt spinning technique. By dissolving away part of the active elements on the surface of the ribbon through a simple and rapid chemical dealloying method to selectively dissolve some active elements on the ribbon's surface, Pt catalysts embedded in the MG support are obtained. Notably, the sample achieved a current density of 1000 mA cm^{-2} at an overpotential of just 102 mV and demonstrated excellent electrochemical stability at high current density (500 mA cm^{-2}). Our experimental results indicate that the modulation of Pt's electronic structure via the MG support optimizes the hydrogen adsorption-free energy of the catalyst through the strong metal-support interaction, thereby enhancing its activity. This type of low-cost, high-efficiency catalyst holds significant promise for industrial applications, offering a sustainable solution for energy conversion.

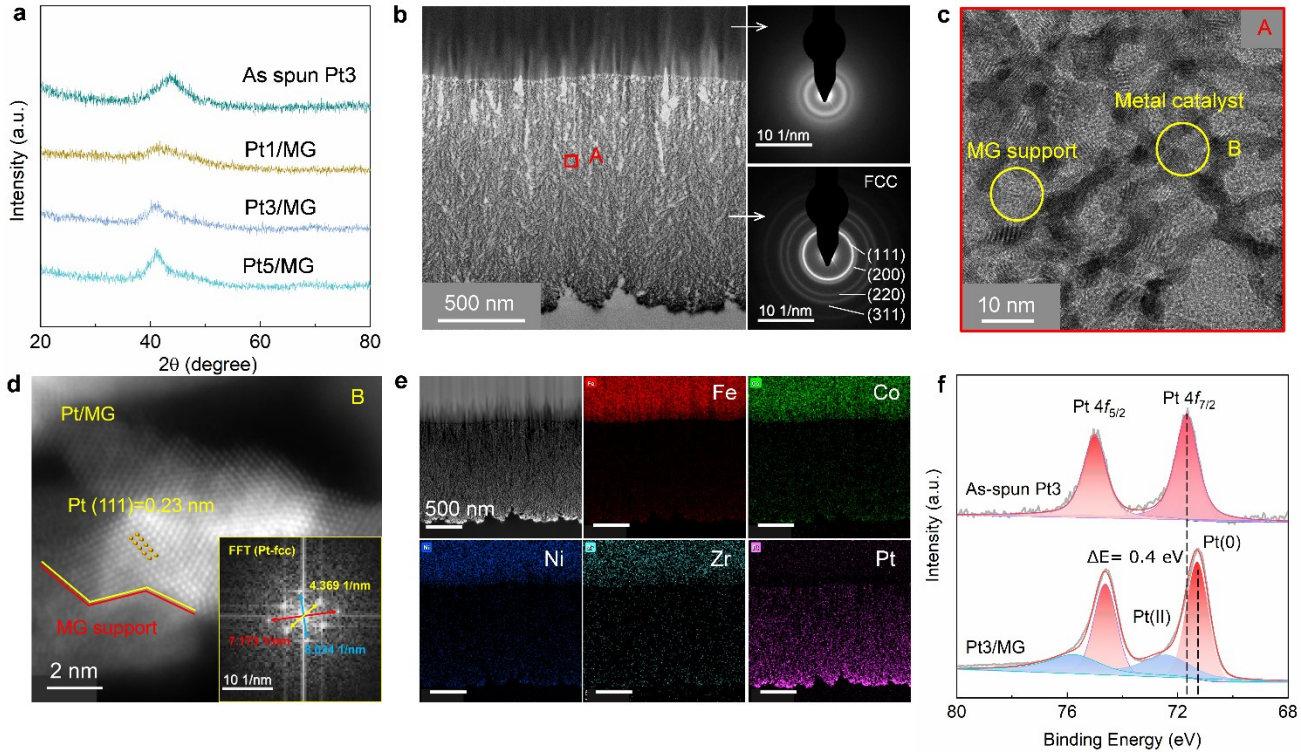

Fig. 2 Structural characterization of the Pt/MG catalysts. (a) XRD patterns of the as-spun ribbon and Pt/MG catalysts. (b) Cross-sectional TEM image of the Pt3/MG catalyst, SAED pattern of MG substrate in the upper right, and SAED pattern of the nanoporous layer in the lower right. (c) The STEM image of the porous layer ribbon, with the fast Fourier transform (FFT) image of the nanocrystalline region shown in the lower right corner. (d) HRTEM image of nanocrystals on the porous layer of Pt3/MG catalyst. (e) Element mapping results of the Pt3/MG catalyst. (f) XPS spectra of Pt 4f in the as-spun Pt3 (up) and Pt3/MG catalyst (down).

Results and Discussion

Synthesis and structures of MG-support Pt catalysts Conclusions

$Fe_{70-x}Co_{10}Ni_{10}Zr_{10}Pt_x$ (x=0, 1, 3, 5) amorphous alloy precursors (as-spun Ptx) were prepared by the melt spinning technique (Experimental details are described in the supplementary information, Fig. 1b). Ribbons with dimensions of 5 m in length, 1 mm in width, and 40 µm in thickness can be produced from the ingot (inset Fig. 1b). The X-ray diffraction (XRD) patterns of the as-spun ribbons, as presented in Fig. S1, exhibit diffused peaks between 2θ = 40-50˚. The absence of any sharp peaks indicates a fully metallic glass state. Pt nanocatalysts loaded on the MG support (Ptx/MG) are finally obtained by chemical dealloying in a 2M H_2SO_4 solution. This process is aimed at increasing the specific surface areas by creating nanoporous layers. The XRD patterns of all the Ptx/MG catalysts show a similar structure to the amorphous alloy precursors, indicating that the samples did not form large crystals (Fig. 2a). After dealloying, there is a significant change in the surface structure. Compared to the flat and smooth surface of the as-spun amorphous alloy precursor (as depicted in Fig. S2a, d, and g), a hierarchically rough surface with nanosized pores was observed (shown in Fig. S2b, e, and h). The thickness of the dealloyed layer is estimated to be about 1.5 µm (Fig. S2c, f, and i). According to the analysis of the $Fe_{70-x}Co_{10}Ni_{10}Zr_{10}Pt_x$ (x=3) (Pt3) series samples, the surface morphology and porosity of the samples are not sensitive to the duration of dealloying, as demonstrated in Fig. S3.

The structure and composition of the Pt/MG support catalysts are elucidated using transmission electron microscopy (TEM). The cross-sectional image (Figure 2b) distinctly reveals that the surface layer, post-dealloying, exhibits a highly porous structure, whereas the inner layer, untouched by etching, remains compact. Selected area electron diffraction (SAED) patterns indicate that while the surface layer is polycrystalline, the inner layer maintains its amorphous metallic glass state. A detailed examination of the porous surface layer uncovers numerous nanoparticles, averaging less than 10 nm in size, intertwined within the MG matrix, as illustrated in Figures 2c and S4. We utilized spherical aberration-corrected transmission electron microscopy (AC-TEM) to further analyse the crystallized nanoparticles. As shown in Figure 2d, the precisely defined lattice fringes, with an interplanar spacing of 0.235 nm, match the (111) plane of the face-centered cubic (fcc) phase of Pt, aligning with the observed fast Fourier transform (FFT) pattern. Elemental mapping across the section reveals the formation of Pt nanoparticles following the extensive dissolution of Fe, Co, Ni, and Zr elements during the dealloying process (Fig. 2e, Fig. S5, and S6).

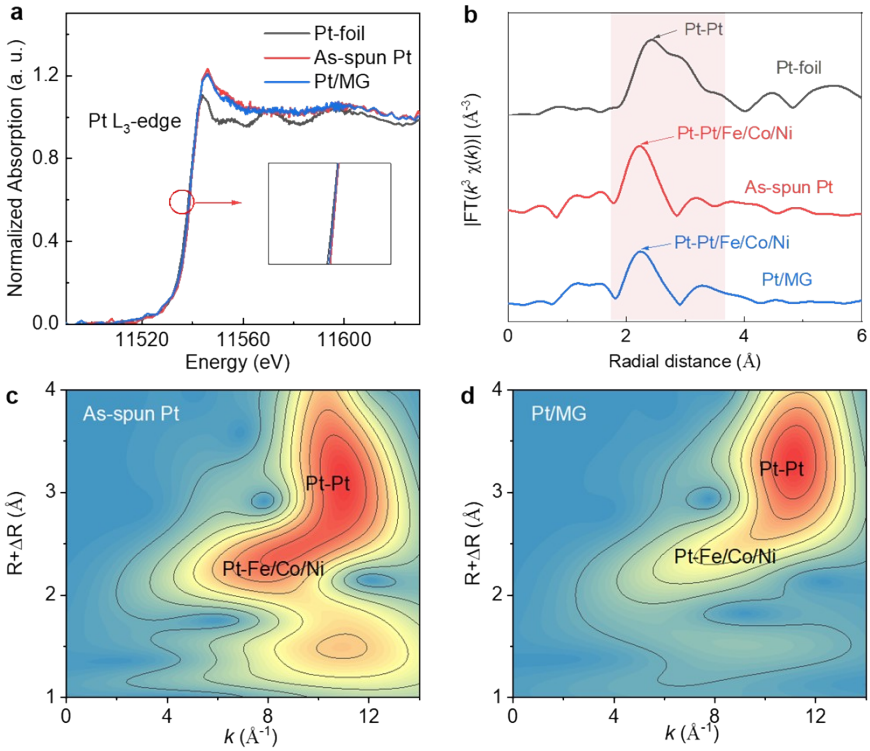

Fig. 3 Electronic Characterization and Analysis. (a) The normalized Pt L3-edge XANES spectra of Pt-foil, As-spun Pt5 and Pt5/MG. (b) Fourier transform of the k^3-weighted Pt L3-edge EXAFS spectra. (c-d) Wavelet transform of the k^3-weighted Pt L3-edge EXAFS results for as-spun Pt5 and Pt5/MG.

The surface electronic structures were investigated by X-ray photoelectron spectroscopy (XPS). XPS spectra of Fe, Ni, Co, Zr, and Pt indicate that all the elements in the as-spun ribbon remain predominantly in metallic states, despite a minor degree of oxidation (Fig. S7).[40, 41] Notably, the binding energies of Fe, Co, and Ni remained almost unchanged after 2 minutes of dealloying, demonstrating the high chemical stability of the metallic glass (MG) support. Most of the Zr is dissolved and oxidized during the dealloying process. Interestingly, there is a detectable positive shift in the binding energy for the Fe 2p (0) peak, moving from 706.81 eV for the MG precursor to 707.65 eV after dealloying (Fig. S7). Conversely, there is a significant negative shift (0.4 eV) for the Pt 4f (0) peak (Fig. 2f). Different Pt loading levels underwent similar changes during the preparation process (Fig. S8). This indicates a significant electron transfer from the iron atoms in the metal-glass support to the platinum nanoparticles, due to the metal-support interaction. This process is vital for adjusting the electronic structures and altering the adsorption/desorption characteristics of Pt catalysts [39, 42] The highly porous structures provide catalysts with a large reactive surface area, and stable metallic glass (MG) support enhances the electron transfer efficiency of the catalyst. Furthermore, the catalyst surface exposes a significant amount of electronically-tuned platinum (Pt), which might markedly improve the catalytic efficiency of the Pt/MG catalyst.

X-ray absorption spectroscopy (XAS) has further elucidated the structure of Pt/MG. The X-ray absorption near-edge structure (XANES) spectra at the Pt L3 edge reveal that the near-edge binding energies of the three materials are similar, indicating that the Pt species in Pt/MG and As-spun Pt largely retain a metallic state structure consistent with that of Pt foil (Fig. 3a), which corroborates the analysis results obtained from XPS.[43] The Fourier-transformed extended X-ray absorption fine structure (EXAFS) spectra (R-space) of the catalysts, displayed in Fig. 3b, reveal the existence of Pt-Pt coordination in both As-spun Pt and Pt/MG. However, due to the significant alloying effect in the metallic glass, Pt is also coordinately bonded with transition metals like Fe in the catalyst, potentially explaining the leftward shift of the Pt-Pt coordination peak in R-space.[44] The wavelet transform spectra (Fig. 3c-d, and Fig. S9) further substantiated this finding. Noteworthy, the EXAFS fitting parameters of the catalyst, presented in Fig. S10 and Table S1, suggest a larger number of Pt-Pt coordinations and fewer Pt-Fe coordinations in the Pt/MG catalyst compared to As-spun Pt. This implies that the Pt nanocrystal clusters in the Pt/MG catalyst are firmly anchored onto the metallic glass support, potentially enabling the catalyst to expose numerous Pt sites while maintaining high electrochemical stability.

Electrochemical Activity of the Pt/MG catalysts

The electrolytic water-splitting activity of the prepared sample was evaluated using a three-electrode system, with a carbon rod serving as the counter electrode in a 1M or 6.9M (30 wt%) KOH alkaline solution. The Pt/MG catalysts demonstrate

remarkably high activities toward the Hydrogen Evolution

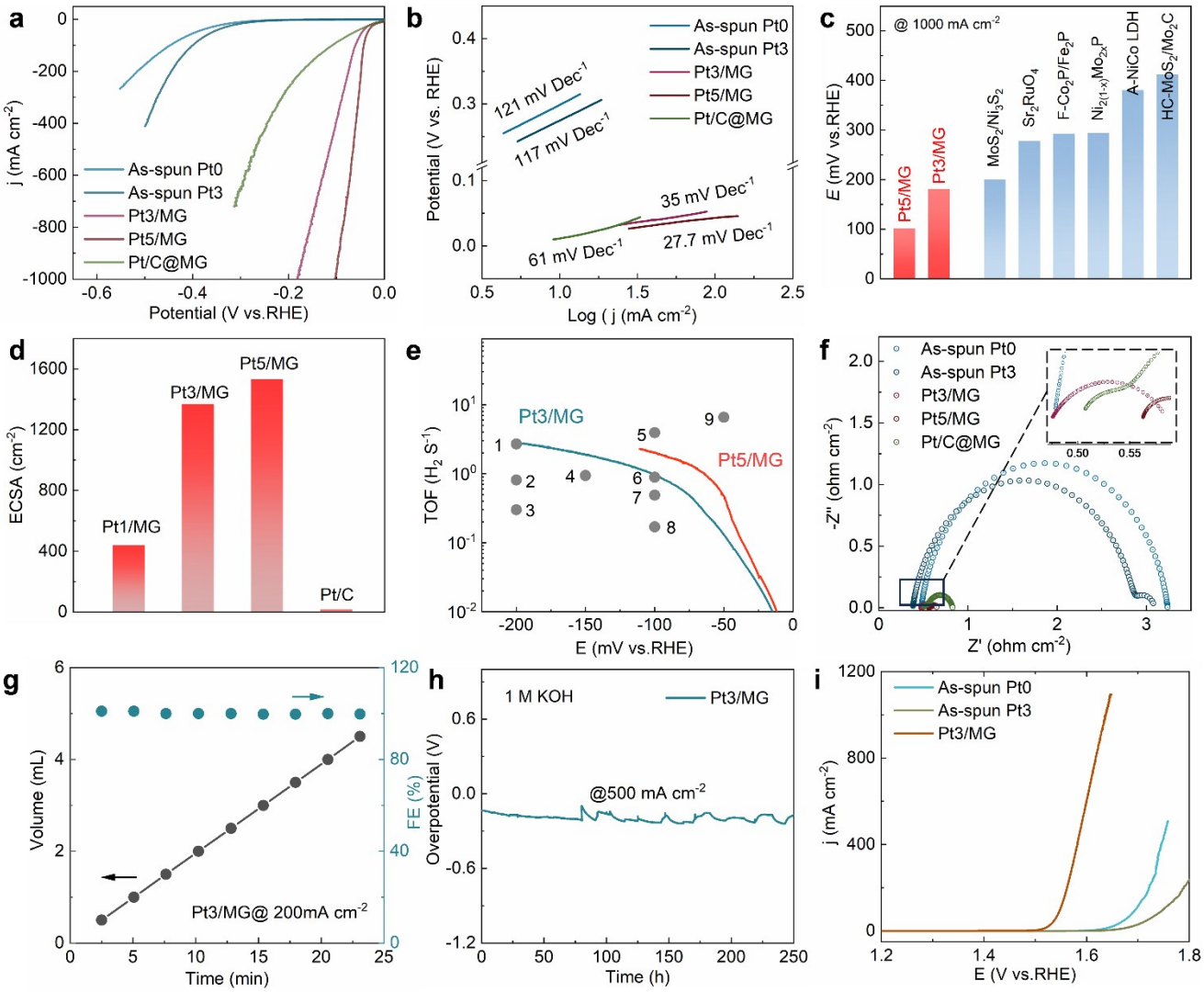

Fig. 4 Electrochemical properties in a 1M KOH alkaline solution of the Pt/MG catalysts. (a) HER Polarization curves of as as-spun Pt0, Pt3, Pt3/MG, Pt5/MG, and Pt/C@MG catalysts. (b) The corresponding Tafel slopes of the catalysts. (c) HER activity with recently reported electrocatalysts at high current densities. (d) ECSA of the Pt1/MG, Pt3/MG, Pt5/MG, and Pt/C@MG catalysts. (e) Comparison of TOF values of the Pt/MG catalysts with recently reported state-of-the-art catalysts. (1. $AlNiYMnCuAu_3$,[45] 2. NiFeCoCuTi,[46] 3. MoS_3,[47] 4. $AlNiYMnCuAu_3$,[45] 5. Pt/np-$Co_{0.85}Ce$,[48, 49] 6. NiZrTiPt,[30] 7. Pt/C,[30] 8. np-$Co_{0.85}Ce$,[48] 9. PdPtCuNiP.[32] (f) Nyquist plots of the Ptx/MG catalysts. (g) Faraday efficiency of Pt3/MG catalyst at a current density of 200 mA cm^{-2}. (h) Long-term stability test of Pt3/MG at a current density of 500 mA cm^{-2} for 250 h. (i) OER polarization curves of the Pt3/MG.

Reaction (HER), as shown in Fig. 4a and Table S3. To achieve a current density of 10 mA cm^{-2}, Pt1/MG, Pt3/MG, and Pt5/MG require overpotentials of 22, 19, and 18 mV respectively. Most importantly, these dealloyed catalysts exhibit high intrinsic catalytic activities, especially when normalized to the electrochemically active surface areas (ECSA) (Figure S11). These values are significantly lower than those of a Pt ribbon (43 mV@10 mA cm^{-2}) and other recently reported noble metal catalysts such as Pt/C60,[27] PdPtCuNiP,[32] Pt@CoS[50] (24, 32, 28 mV@10 mA cm^{-2}) (Fig. S12d, Table S3). The observed overpotentials are also much lower than those of the corresponding amorphous alloy precursors, underscoring the crucial influence of the dealloying procedure. It is also noted that the catalytic activities are strongly dependent on dealloying times, as illustrated in Fig. S12-S14. For the Pt5/MG catalyst, the overpotential decreases from 23 to 18 mV when the dealloying time is increased from 1 to 3 minutes (Fig. S14a). Generally, a longer dealloying time increases the porosity and specific surface areas of the MG support, thereby enhancing HER performance.[44] Remarkably, all the MG-supported catalysts are capable of delivering a high current density of 1000 mA cm^{-2} at relatively low overpotentials, such as 181 mV for Pt3/MG, and 102 mV for Pt5/MG, and outperforming most currently developed electrocatalysts (Fig. 4c). As shown in Fig. 4b, the Tafel slopes for the Pt3/MG and Pt5/MG are determined to be 35 and 27.7 mV dec^{-1}, respectively, implying that the rate-determining step should be the hydrogen desorption process.[37] In alkaline environments, electronically structured-modified Pt serves as active sites, displaying strong hydrolysis dissociation

ability, thereby greatly enhancing the efficiency of hydrogen

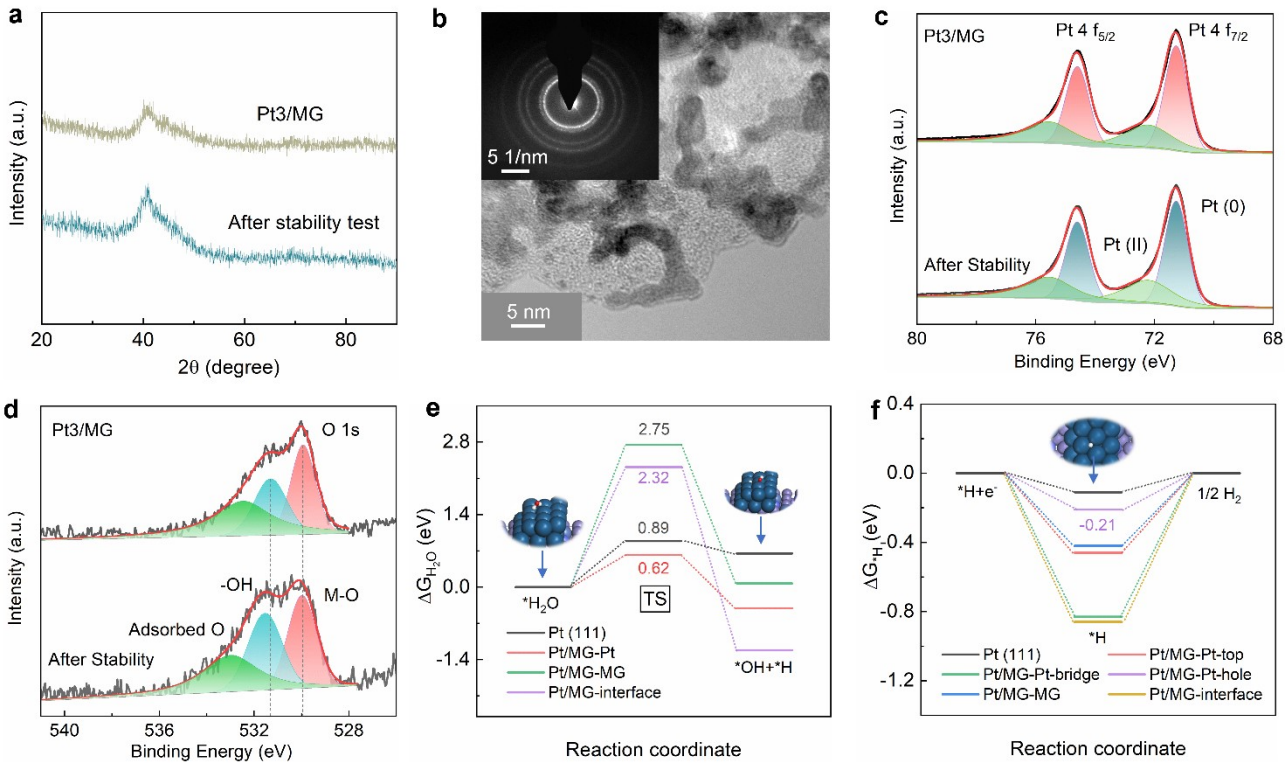

Fig. 5 The structure and catalytic mechanism of the Pt/MG. (a) XRD patterns of Pt3/MG catalyst samples before and after long-term stability test. (b) HRTEM images of Pt3/MG catalyst samples before and after the stability test, the selected area diffraction pattern of the porous layer in the upper left corner of b. (c-d) XPS spectrum of Pt 4f and O 1s in the Pt3/MG catalyst after HER and stability test corresponding to Pt 4f and O 1s. (e-f) The water dissociation energy berries and the Gibbs free energy diagram of the Pt/MG and Pt (111).

evolution.[51, 52]

The electrochemical surface area (ECSA) of the sample reflects the number of active sites involved in the electrochemical reaction.[53] The samples prepared by the dealloying method could have a high ECSA. In this study, the double layer capacitance (C_{dl}) of the Pt3/MG catalyst is measured to be 54.79 mF cm^{-2} by scanning the non-Faradaic region of the sample (Fig. S15-17). This results in an ECSA of 1369 cm^2, suggesting a substantial exposure of reactive sites with MG as support (Fig. 4d). The turnover frequency (TOF) of the catalysts is determined from the ECSA by assuming that all the Pt atoms in the porous layer are active for HER.[54] At an overpotential of 100 mV, the TOF values for Pt3/MG and Pt5/MG are determined to be 0.975 S^{-1} and 2.053 S^{-1}, respectively (Fig. 4e). These values are much higher than many of recent report state-of-the-art-noble catalysts, including Pt/C,[27] NiZrTiPt,[30] Ru@SC-CDs,[55] Pd/C,[56] (1.5, 0.89, 0.1, 0.44 S^{-1}), *etc* (Table S5). suggesting the high intrinsic activities of the Pt/MG catalysts. Electrochemical impedance spectroscopy (EIS) is utilized to analyse the reaction kinetics and electron transfer behaviors (Fig. 4f). The Nyquist plots reveal that the solution resistance (R_s) and the charge transfer resistance (R_{ct}) of the Pt3/MG catalyst are 0.47 ohm cm^{-2} and 0.11 ohm cm^2, respectively, which are significantly lower than those of the Pt/C@MG (0.54 ohm cm^{-2} and 0.29 ohm cm^{-2}). These lower resistances indicate that the high conductivity of the MG support, along with the strong chemical bonding between Pt and MG support, enhances the electron transfer kinetics during the HER. Moreover, the enrichment of Pt sites with high catalytic activity on the sample surface results in low internal resistance, fast charge transfer behavior and fast HER kinetics.

In addition, the sample exhibits a remarkable energy conversion efficiency. The Faraday efficiency of the Pt3/MG catalyst was tested at a current density of 200 mA cm^{-2} and found to be close to 100%. (Fig. 4g). Durability is a key factor in assessing catalysts, and Pt3/MG showcases significant stability, preserving its effectiveness after 250 hours of testing at a high current density of 500 mA cm^{-2} (see Fig. 4h), before an increase to 1000 mA cm^{-2} is observed (Fig. S18). Furthermore, the catalyst exhibits sustained stability over 220 hours of continuous operation in 6.9 M KOH electrolyte that close to the industrial operations (Fig. S19). Notably, the Pt nanocrystals demonstrate robust resistance to oxidation following the stability test, as indicated by the Pt (0) states in X-ray Photoelectron Spectroscopy (XPS) results (Fig. S20). After 2000 cycles of cyclic voltammetry (CV), the catalyst still maintains an overpotential of 184 mV at 1000 mA cm^{-2} (Fig. S18a). Most importantly, there are no significant changes to the porous structures, indicating the high mechanical strength of the metallic glass (MG) support (Fig. S21b). Finally, it is found that the Pt/MG could be a bifunctional electrocatalyst for water splitting. When used as a catalyst for oxygen evolution reaction,

it only requires an overpotential of 280mV to reach a current density of 10mA cm^{-2}, together with a low Tafel slope of only 26.8 mV dec^{-1} (Fig. 4i, S22), and the R_{ct} of it is 0.07 ohms cm^{-2}. These results indicate the potential of the samples for commercial alkaline water splitting.

Understanding the role of MG support

To shed light on the high activity and stability of MG-supported Pt catalysts, we examined the XRD patterns of Pt3/MG catalyst samples after conducting durability tests for 250 hours at a current density of 500mA cm^{-2}. These patterns, compared with those of the freshly prepared samples (Fig. 5a), showed no discernible structural alterations. The presence of a broad peak indicates the absence of crystallization or growth in crystal size throughout the catalytic reactions, suggesting a stable phase. Notably, the atomic ratios between Fe, Co, and Ni remained nearly unchanged, which is crucial for maintaining the catalyst's activity. Particularly compelling is the observation that the atomic ratio of Pt did not significantly decrease, implying a robust bonding between Pt and the MG support that effectively prevents Pt detachment under harsh reaction conditions (Fig. S23, Table S6). The high-resolution TEM (HRTEM) image of the samples before and after the test shows that the size of the nanograins is not changed by the prolonged test, as shown in Fig. 5b. These results collectively indicate that the porous samples, prepared by dealloying MG with Pt loading, maintain high structural stability without significant Pt detachment, nanocrystalline grain growth, or agglomeration.

X-ray Photoelectron Spectroscopy (XPS) was employed to monitor the changes in the surface electronic structures and the chemical valence states of the Pt3/MG catalysts, as depicted in Fig. S24. It was surprising to observe that the binding energies for the Fe, Co, and Ni elements remained nearly constant following both the Hydrogen Evolution Reaction (HER) testing and stability assessments. All these elements retained their metallic (0) states, indicating minimal alteration in their electronic environment. For the Pt atoms, which serve as the primary catalytic active sites, there was no significant shift in the binding energy of their metallic state, with only a minor indication of Pt oxidation (Fig. 5c). This observation underscores the excellent antioxidative capacity of both the metallic glass (MG) support and the Pt metal catalysts, suggesting their robustness and stability under the conditions tested. The O 1s spectra were investigated to uncover the chemical states and electronic structure of the adsorbed oxygen species at the surface (Fig. 5d). The peaks at binding energies of 529.8, 531.4, and 533 eV can be assigned to metal-O bonds, surface-absorbed hydroxyl group, and adsorbed water molecular, respectively.[57] The high percentage of surface-absorbed hydroxyl group coverage may improve the formation of the O-O bond in -OOH group, which is beneficial for the OER processes.[57, 58]

Electron transfer between the Pt catalyst and the MG support can be harnessed to adjust the electronic structure of Pt, thereby enhancing its electrocatalytic performance, and the DFT calculations have elucidated the mechanism of its activity. These calculations are based on a model comprising Pt nanocrystal loaded onto MG layer, derived from the Pt3/MG structural framework, with the Pt (111) face exposed. In alkaline environments, the dissociation of water is typically the key rate-limiting step in the Hydrogen Evolution Reaction (HER).[59, 60] Following the search for the water dissociation transition state, the energy barrier for breaking the OH-H bond on the Pt (111) surface stands at 0.89 eV, whereas for Pt supported on MG, the barrier for water dissociation is merely 0.62 eV, also significantly lower than that on the Pt/MG-MG layer and the Pt/MG-interface (see Fig. 5e, Fig. S25).[61, 62] Thus, the Pt/MG-Pt (111) significantly facilitates the dissociation of water. Additionally, at the Pt hole sites, the catalyst exhibits Gibbs free energy of *H (ΔG_{*H}) which is quite low (illustrated in Fig. 5f, Table S7). The exposure of a multitude of highly active Pt sites within Pt/MG promotes the adsorption and desorption of hydrogen, rendering the Tafel step the dominant factor in the HER process.[42, 63-65] Although the percentage of negatively charged Pt atoms, which serve as the catalytically active sites for water dissociation, strongly depends on the size of the nanoparticle and is generally limited to the surface close to the support, it is sufficient to influence the electronic structures and catalytic activities of the metal nanoparticles. This is because the critical size for the dominance of electronic effects could be up to several nanometers, thereby influencing the adsorption/desorption behaviors of reaction intermediates.[66, 67] This work demonstrates how metal-support interaction and electronic structure regulation are pivotal in enhancing catalytic performance.

Conclusions

In summary, we've developed a novel type of metallic glass (MG) support for metal catalysts using a fast and efficient dealloying method based on amorphous alloy precursors. Compared to the commonly utilized carbon supports, the MG support offers superior mechanical stability, heightened electrical conductivity, increased specific surface areas, and exceptional chemical stability that effectively resists oxidation. Furthermore, the robust metal-support interaction between the MG support and the metal catalysts can modify the electronic structures of Pt catalysts, optimizing adsorption behaviors. Consequently, Pt3/MG catalysts post-dealloying exhibit an impressively low overpotential of just 181 mV at a current density of 1000 mA cm^{-2} and maintain impressive stability, even after 250 hours of operation at 500 mA cm^{-2}. This research introduces a promising avenue for creating cost-effective catalysts with enhanced catalytic performance.

Author Contributions

Mengqi Pan data curation, investigation, methodology, validation, writing-original draft; **Heyang Feng** data curation, writing-review& editing; **Ziyong Zhang** data curation, methodology; **Meng Gao** supervision, validation, editing; **Lei Lei** data curation; **Degao Wang** data curation; **Guowei Li** conceptualization, supervision, writing-review & editing; **Juntao Huo** conceptualization, supervision, writing-

review & editing; **Jun-Qiang Wang** conceptualization, supervision, writing-review & editing, Funding Acquisition.

Conflicts of interest

There are no conflicts to declare.

Acknowledgements

The authors acknowledge the financial supports from the National Key R&D Program of China (2018YFA0703600), National Natural Science Foundation of China (NSFC 52222105, 51827801, 52071327, 92163108, 52271194), Youth Innovation Promotion Association CAS (No. 2019296), Ningbo Yongjiang Talent Introduction Programme (2022A-090-G), the Max Planck Partner Group program, the Hundred Talents Programs in Chinese Academy of Science, and Zhejiang Provincial Natural Science Foundation of China (LR22E010004, 2022C01023).

Notes and references

1. I. Staffell, D. Scamman, A. Velazquez Abad, P. Balcombe, P. E. Dodds, P. Ekins, N. Shah and K. R. Ward, *Energy Environ. Sci.*, 2019, **12**, 463-491.
2. J. A. Turner, *Science*, 2004, **305**, 972-974.
3. J. Yang, A. R. Mohmad, W. Yan, R. Fullon, X. J. Song, F. Zhao, I. Bozkurt, M. Augustin, E. J. G. Santos, H. S. Shin, W. J. Zhang, D. Voiry, H. Y. Jeong and M. Chhowalla, *Nat. Mater.*, 2019, **18**, 1309–1314
4. P. Ruan, B. Chen, Q. Zhou, H. Zhang, Y. Wang, K. Liu, W. Zhou, R. Qin, Z. Liu, G. Fu and N. Zheng, *The Innovation*, 2023, **4**, 100362.
5. X. Li, Y. Chen, X. Zhan, Y. Xu, L. Hao, L. Xu, X. Li, M. Umer, X. Tan, B. Han, A. W. Robertson and Z. Sun, *The Innovation Materials*, 2023, **1**, 100014.
6. J.-a. Lai, Z. Zhang, X. Yang and Y. Zhang, *The Innovation Materials*, 2023, **1**, 100020.
7. N. Daelman, M. Capdevila-Cortada and N. López, *Nat. Mater.*, 2019, **18**, 1215-1221.
8. Q. Yang, Y. Zhang, Y. Sun, C. Felser and G. Li, *The Innovation Materials*, 2023, **1**, 100013.
9. C. Xu, R. Wang, M. Chen, Y. Zhang and Y. Ding, *Phys. Chem. Chem. Phys.*, 2010, **12**, 239-246.
10. R. Wang, C. Xu, X. Bi and Y. Ding, *Energy Environ. Sci.*, 2012, **5**, 5281-5286.
11. H. Liu, X. H. Zhang, Y. X. Li, X. Li, C. K. Dong, D. Y. Wu, C. C. Tang, S. L. Chou, F. Fang and X. W. Du, *Adv. Energy Mater.*, 2020, **10**, 1902521.
12. B. Huang, Y. Ma, Z. Xiong, W. Lu, R. Ding, T. Li, P. Jiang and M. Liang, *Sustain. Energ. Fuels*, 2020, **4**, 3288-3292.
13. F. Guo, T. J. Macdonald, A. J. Sobrido, L. Liu, J. Feng and G. He, *Adv. Sci.*, 2023, **10**, 2301098.
14. M. Zhang, J. Guan, Y. Tu, S. Wang and D. Deng, *The Innovation*, 2021, **2**, 100144.
15. S. Zaman, M. Wang, H. J. Liu, F. M. Sun, Y. Yu, J. L. Shui, M. Chen and H. J. Wang, *Trends Chem*, 2022, **4**, 886-906.
16. Y. Sun, S. Polani, F. Luo, S. Ott, P. Strasser and F. Dionigi, *Nat. Commun.*, 2021, **12**, 5984.
17. S. K. Kaiser, Z. Chen, D. Faust Akl, S. Mitchell and J. Pérez-Ramírez, *Chem. Rev.*, 2020, **120**, 11703-11809.
18. R. Gao, J. Wang, Z.-F. Huang, R. Zhang, W. Wang, L. Pan, J. Zhang, W. Zhu, X. Zhang, C. Shi, J. Lim and J.-J. Zou, *Nat. Energy*, 2021, **6**, 614-623.
19. W. H. Wang, *Prog. Mater Sci.*, 2019, **106**, 100561.
20. J. Huo, K. Li, B. Zang, M. Gao, L.-M. Wang, B. Sun, M. Li, L. Song, J.-Q. Wang and W.-H. Wang, *Chin. Phys. Lett.*, 2022, **39**, 046401.
21. J. S. Sun, Z. Wen, L. P. Han, Z. W. Chen, X. Y. Lang and Q. Jiang, *Adv. Funct. Mater.*, 2018, **28**, 1706127.
22. J. Wang, L. Song, Y. Gao, B. Zang, M. Gao, J. Huo, L. Hu and J.-Q. Wang, *Sci. China Mater.*, 2023, **66**, 3706-3712.
23. S. Anantharaj and S. Noda, *Small*, 2020, **16**, e1905779.
24. S. Ju, J. Feng, P. Zou, W. Xu, S. Wang, W. Gao, H.-J. Qiu, J. Huo and J.-Q. Wang, *J. Mater. Chem. A*, 2020, **8**, 3246-3251.
25. L.-C. Zhang, Z. Jia, F. Lyu, S.-X. Liang and J. Lu, *Prog. Mater Sci.*, 2019, **105**, 100576.
26. H.-J. Qiu, G. Fang, Y. Wen, P. Liu, G. Xie, X. Liu and S. Sun, *J. Mater. Chem. A*, 2019, **7**, 6499.
27. J. Chen, M. Aliasgar, F. B. Zamudio, T. Zhang, Y. Zhao, X. Lian, L. Wen, H. Yang, W. Sun, S. M. Kozlov, W. Chen and L. Wang, *Nat. Commun.*, 2023, **14**, 1711.
28. Y. C. Hu, Y. W. Li, Y. Yang, P. F. Guan, H. Y. Bai and W. H. Wang, *Proc. Natl. Acad. Sci. U.S.A.*, 2018, **115**, 6375-6380.
29. X. Y. Lang, G. F. Han, B. B. Xiao, L. Gu, Z. Z. Yang, Z. Wen, Y. F. Zhu, M. Zhao, J. C. Li and Q. Jiang, *Adv. Funct. Mater.*, 2014, **25**, 230-237.
30. R. Li, X. Liu, R. Wu, J. Wang, Z. Li, K. C. Chan, H. Wang, Y. Wu and Z. Lu, *Adv. Mater.*, 2019, **31**, e1904989.
31. Y. C. Hu, Y. Z. Wang, R. Su, C. R. Cao, F. Li, C. W. Sun, Y. Yang, P. F. Guan, D. W. Ding, Z. L. Wang and W. H. Wang, *Adv. Mater.*, 2016, **28**, 10293-10297.
32. Z. Jia, K. Nomoto, Q. Wang, C. Kong, L. Sun, L. C. Zhang, S. X. Liang, J. Lu and J. J. Kruzic, *Adv. Funct. Mater.*, 2021, **31**, 2101586.
33. L. Li, Y. Liu, B. Lin, Y. Wang, K. Song, H. Zhang, Y. Li, J. Li, H. Zheng, J. Tang, Z. Yu and J. Qiao, *Int. J. Hydrogen Energy*, 2023, **48**, 27182-27200.
34. P. C. K. Vesborg, B. Seger and I. Chorkendorff, *J. Phys. Chem. Lett.*, 2015, **6**, 951-957.
35. M. Carmo, D. L. Fritz, J. Mergel and D. Stolten, *Int. J. Hydrogen Energy*, 2013, **38**, 4901-4934.
36. K. Zeng and D. Zhang, *Prog. Energy Combust. Sci.*, 2010, **36**, 307-326.
37. Y. Zhang, K. E. Arpino, Q. Yang, N. Kikugawa, D. A. Sokolov, C. W. Hicks, J. Liu, C. Felser and G. Li, *Nat Commun*, 2022, **13**, 7784.
38. Z. C. L. H.X. Lia, S.L. Wangb, Y. Wua, Z.P. Lua, *Prog. Mater Sci.*, 2019, **103**, 235-318.
39. J. Tian, Y. Rao, W. Shi, J. Yang, W. Ning, H. Li, Y. Yao, H. Zhou and S. Guo, *Angew. Chem. Int. Ed.*, 2023, **62**, e202310894.
40. Z. Li, R. Ma, Q. Ju, Q. Liu, L. Liu, Y. Zhu, M. Yang and J. Wang, *The Innovation*, 2022, **3**, 100268.
41. D. Lai, Q. Kang, F. Gao and Q. Lu, *J. Mater. Chem. A*, 2021, **9**, 17913-17922.
42. J. Kwon, S. Sun, S. Choi, K. Lee, S. Jo, K. Park, Y. K. Kim, H. B. Park, H. Y. Park, J. H. Jang, H. Han, U. Paik and T. Song, *Adv. Mater.*, 2023, **35**, 2300091.
43. J. Shi, C.-w. Kao, J. Lan, K. Jiang, M. Peng, M. Luo, Y.-R. Lu, S. Zhang and Y. Tan, *J. Mater. Chem. A*, 2023, **11**, 11526.
44. X. Zhang, Y. Yang, Y. Liu, Z. Jia, Q. Wang, L. Sun, L. C. Zhang, J. J. Kruzic, J. Lu and B. Shen, *Adv. Mater.*, 2023, **35**,

2303439.
45. P. Zou, B. Zang, L. Song, W. Xu, J. Huo and J.-Q. Wang, *ACS Appl. Nano Mater.*, 2022, **5**, 17673-17681.
46. H. Shi, X.-Y. Sun, S.-P. Zeng, Y. Liu, G.-F. Han, T.-H. Wang, Z. Wen, Q.-R. Fang, X.-Y. Lang and Q. Jiang, *Small Struct.*, 2023, **4**, 2300042.
47. J. D. Benck, Z. Chen, L. Y. Kuritzky, A. J. Forman and T. F. Jaramillo, *ACS Catal.*, 2012, **2**, 1916-1923.
48. K. Jiang, B. Liu, M. Luo, S. Ning, M. Peng, Y. Zhao, Y.-R. Lu, T.-S. Chan, F. M. F. de Groot and Y. Tan, *Nat. Commun.*, 2019, **10**, 1743.
49. Y. Yan, C. Wang, Z. Huang, J. Fu, Z. Lin, X. Zhang, J. Ma and J. Shen, *J. Mater. Chem. A*, 2021, **9**, 5415-5424.
50. A. Mosallanezhad, C. Wei, P. Ahmadian Koudakan, Y. Fang, S. Niu, Z. Bian, B. Liu, T. Huang, H. Pan and G. Wang, *Appl. Catal. B Environ.*, 2022, **315**, 121534.
51. K. Liu, H. Yang, Y. Jiang, Z. Liu, S. Zhang, Z. Zhang, Z. Qiao, Y. Lu, T. Cheng, O. Terasaki, Q. Zhang and C. Gao, *Nat. Commun.*, 2023, **14**, 2424.
52. F. Guo, Z. Zhang, R. Chen, Y. Tan, W. Wu, Z. Wang, T. Zeng, W. Zhu, C. Lin and N. Cheng, *Materials Horizons*, 2023, **10**, 2913-2920.
53. Q. Yang, G. Li, K. Manna, F. Fan, C. Felser and Y. Sun, *Adv. Mater.*, 2020, **32**, 1908518.
54. G. W. Li, S. Khim, C. S. Chang, C. G. Fu, N. Nandi, F. Li, Q. Yang, G. R. Blake, S. Parkin, G. Auffermann, Y. Sun, D. A. Muller, A. P. Mackenzie and C. Felser, *ACS Energy Lett.*, 2019, **4**, 2185-2191.
55. Y. Liu, Y. Yang, Z. Peng, Z. Liu, Z. Chen, L. Shang, S. Lu and T. Zhang, *Nano Energy*, 2019, **65**, 104023.
56. Y. Zheng, Y. Jiao, Y. Zhu, L. H. Li, Y. Han, Y. Chen, M. Jaroniec and S.-Z. Qiao, *J. Am. Chem. Soc.*, 2016, **138**, 16174-16181.
57. Y. Zhang, Y. Wang, W. Sun, D. Ma, J. Ma, J. Rao, Q. Xu, J. Huo, J. Liu and G. Li, *Adv. Mat. Interfaces*, 2023, **10**, 2300279.
58. D. Strmcnik, P. P. Lopes, B. Genorio, V. R. Stamenkovic and N. M. Markovic, *Nano Energy*, 2016, **29**, 29-36.
59. T. Ma, H. Cao, S. Li, S. Cao, Z. Zhao, Z. Wu, R. Yan, C. Yang, Y. Wang, P. A. van Aken, L. Qiu, Y. G. Wang and C. Cheng, *Adv. Mater.*, 2022, **34**, 2206368.
60. Y. Jiang, X. Q. Wu, Y. C. Yan, S. Luo, X. Li, J. B. Huang, H. Zhang and D. R. Yang, *Small*, 2019, **15**, 1805474.
61. P. Wang, X. Zhang, J. Zhang, S. Wan, S. Guo, G. Lu, J. Yao and X. Huang, *Nat. Commun.*, 2017, **8**, 14580.
62. G. W. Li, C. G. Fu, W. J. Shi, L. Jiao, J. Q. Wu, Q. Yang, R. Saha, M. E. Kamminga, A. K. Srivastava, E. K. Liu, A. N. Yazdani, N. Kumar, J. Zhang, G. R. Blake, X. J. Liu, M. Fahlman, S. Wirth, G. Auffermann, J. Gooth, S. Parkin, V. Madhavan, X. L. Feng, Y. Sun and C. Felser, *Angew Chem Int Edit*, 2019, **58**, 13107-13112.
63. S. Jiao, X. Fu and H. Huang, *Adv. Funct. Mater.*, 2021, **32**, 2107651.
64. S. J. Yoo, H. Y. Park, T. Y. Jeon, I. S. Park, Y. H. Cho and Y. E. Sung, *Angew. Chem.*, 2008, **120**, 9447-9450.
65. J. N. Guo, J. L. Liu, X. X. Zhang, X. Y. Guan, M. H. Zeng, J. R. Shen, J. N. Zou, Q. Z. Chen, T. Wang and D. Qian, *J. Mater. Chem. A*, 2022, **10**, 13727-13734.
66. Y. Lykhach, S. M. Kozlov, T. Skála, A. Tovt, V. Stetsovych, N. Tsud, F. Dvořák, V. Johánek, A. Neitzel, J. Mysliveček, S. Fabris, V. Matolín, K. M. Neyman and J. Libuda, *Nat. Mater.*, 2015, **15**, 284-288.
67. Z. Wang, C. Wang, S. Mao, B. Lu, Y. Chen, X. Zhang, Z. Chen and Y. Wang, *Nat. Commun.*, 2022, **13**, 3561.